Dental Materials (2005) **21**, 811–822

dental materials

www.intl.elsevierhealth.com/journals/dema

The crystallization of an aluminosilicate glass in the K_2O-Al_2O_3-SiO_2 system

Michael J. Cattell[a,*], Thomas C. Chadwick[d], Jonathan C. Knowles[c], Richard L. Clarke[b]

[a]*Centre for Adult Oral Health, Bart's and the London, Queen Mary's School of Medicine and Dentistry, Turner Street, Whitechapel, London, E1 2AD, UK*
[b]*Department of Biomaterials in Relation to Dentistry, Queen Mary, University of London, Mile End Road, London E1 4NS, UK*
[c]*Division of Biomaterials and Tissue Engineering, Eastman Dental Institute, University College London, 256 Gray's Inn Road, London WC1X 8LD, UK*
[d]*496 Alegre Avenue, Nipomo, CA 93444, USA*

Received 16 December 2004; accepted 2 February 2005

KEYWORDS
Ceramics;
Leucite;
Crystallization;
Microscopy;
X-ray diffraction

Summary *Objectives*. The aims of the study were to explore the nucleation and crystallization kinetics of an aluminosilicate glass in K_2O–Al_2O_3–SiO_2 system and to characterize it.
Objectives. A starting glass composition of wt%; 64.2% SiO_2, 16.1% Al_2O_3, 10.9% K_2O, 4.3% Na_2O, 1.7% CaO, 0.5% LiO and 0.4% TiO_2 was heated in an electric furnace and later quenched to produce glasses. The glass powders were heat treated using differing heat treatment schedules and quenched. Dta, Xrd, Eds and Sem analyses were used to characterize and explore the crystallization kinetics of the glasses.
Results. Phase separation of the glasses was identified and characterized in the glasses. Tetragonal leucite, cubic leucite and sanadine glass-ceramics were produced. Fine leucite crystals (1 μm^2) were crystallized with minimal matrix microcracking.
Significance. Amorphous phase separation appeared to be an important precursor to nucleation and crystal growth in the alkali aluminosilicate glasses explored. It was possible to control the crystallization of tetragonal leucite and sanidine phases by selected heat treatment of glass powders and monoliths, resulting in the production of fine grained tetragonal leucite glass-ceramics.

Introduction

Leucite containing porcelains are used in dentistry to fabricate dental restorations in order to achieve thermal compatibility when bonding to metallic

* Corresponding author. Tel.: +44 2073777000x2160; fax: +44 2088101254.
E-mail address: m.cattell@qmul.ac.uk (M.J. Cattell).

0109-5641/$ - see front matter © 2005 Academy of Dental Materials. Published by Elsevier Ltd. All rights reserved.
doi:10.1016/j.dental.2005.02.001

substructures and as a reinforcing agent in all ceramic restorations. Leucite glass-ceramics are extremely versatile as they can be processed into dental prostheses via many mechanisms including, sintering, [1] heat pressing [2] and Computer aided design and machining [3].

Depending on the composition, feldspars can be heated to form a eutectic mixture of leucite and liquid according to the K_2O-Al_2O_3-SiO_2 ternary phase diagram [4]. The crystallization of leucite has also been achieved in these glasses by changes to the compositional ratios and an increase in K_2O content, together with the addition of suitable nucleating agents [5]. Significant crystallization was thought to be related to a minimum 1 wt% CaO and at least 12 wt% K_2O content in the glasses [6]. Leucite glass-ceramics can be produced by controlled crystallization of a glass via heat treatments; [7] the addition of synthetic leucite to powdered glass [8] and the blending of a high expansion leucite containing frit with a low expansion glass frit [9].

Leucite ($KAlSi_2O_6$) is a naturally occurring potassium alumino-silicate that has corner linked four and six-membered rings of SiO_4 tetrahedra, forming the structure of a (Si, Al)-O framework silicate. Within the framework formed exists two different cation sites. The larger site contains 16 positions coordinated by 12 oxygens, organized in line with channels formed by six-membered rings. The second site contains 24 positions coordinated by six oxygens, although only 16 are filled [10]. The larger sites are usually occupied by potassium, rubidium or cesium ions and smaller sites by water molecules or left vacant. Cubic and tetragonal leucite both contain 16 ($KAlSi_2O_6$) in the unit cell, with potassium ions occupying the centre of channels aligned in rows parallel to the channel axes in cubic leucite. A reversible temperature dependent cubic to tetragonal leucite phase transformation occurs around 605–625 °C [10,11]. At lower temperatures the potassium ions are too small to fill the cavities in the cubic structure and are moved away from their positions [12]. There is a collapse of the framework about them resulting in a change in symmetry and strain induced crystal twinning [13]. Leucite transformation leads to a reversible 1.2% discontinuous volume change, from low temperature tetragonal to the high temperature cubic leucite starting at 400 °C, in respect to crystallized feldspathic glasses. Lattice parameters for room temperature tetragonal leucite were reported at $a=13.197$ Å (13.197×10^{-10} m) and $c=13.819$ Å (13.819×10^{-10} m) and at 400 °C lattice constraints of $a=13.565$ Å (13.565×10^{-10} m) for cubic leucite. A change in thermal expansion from 22.3×10^{-6}/°C for tetragonal leucite (25–400 °C) to 21.5×10^{-6}/°C for cubic leucite (400–700 °C) is associated with the volume increase [14]. Thermal expansions of $11.7\text{–}12.8\times10^{-6}$/°C (25–600 °C) for cubic leucite [15] and 25×10^{-6}/°C for tetragonal leucite [16] were also reported in the literature, with lattice parameters of $a=13.43$ Å (13.43×10^{-10} m) for cubic leucite (25 °C) [15]. The crystallization or introduction of a high expansion tetragonal leucite phase into a base glass is advantageous to increase its expansion coefficient to a level sufficient to allow efficient bonding to metals. The difference in thermal expansion between the tetragonal leucite crystals and the glassy matrix (8.6×10^{-6}/°C) also provides tangential compressive stresses around the crystals, that is thought responsible for significant strengthening in feldspathic dental porcelain [17].

Typical leucite volume fractions for leucite containing dental porcelains vary between 17 and 45% of tetragonal leucite in a glassy matrix [18,19]. Multiple firings, isothermal heat treatments and cooling of dental porcelains necessary for restoration fabrication can however, modify this content [19–21]. Many of the current commercial porcelain production methods produce dental porcelain with larger leucite crystal sizes (~10 μm) and in some instances more dendritic crystal morphologies [22–24]. The thermal expansion mismatch between the leucite crystals and the glass matrix developed during leucite transformation often causes signs of microcracking around larger (~10 μm), non-uniform leucite crystals and clusters [24–26]. The nucleation and crystallization of aluminosilicate glasses in K_2O-Al_2O_3-SiO_2 system is hence important to study, to control the leucite morphology, distribution, volume fraction and thermal expansion, which is thought to influence the mechanical and wear characteristics of these glass-ceramics [23,27,28]. The aims of the study were therefore to explore the nucleation and crystallization kinetics of an aluminosilicate glass in K_2O-Al_2O_3-SiO_2 system and to characterize it.

Materials and methods

Preparation of the experimental glasses

The composition of the starting glasses selected for this study were wt%; 64.2% SiO_2, 16.1% Al_2O_3, 10.9% K_2O, 4.3% Na_2O, 1.7% CaO, 0.5% LiO and 0.4% TiO_2 [7]. The glass components were ground (74 μm sieve size), placed in a baffle jar and agitated on a jar roll to mix the ingredients for 2 h. The mixed batch

(355105) was transferred to an alumina lined cordierite sagger and heated in an electric kiln (Fredrickson Kiln Co., New York, USA) at 10 °C/min to 1250 °C, held for 4 h and then removed and allowed to air cool in the furnace. A second glass was also made using the same components as batch 355105 but was heated in a platinum crucible in an electric furnace (RHF 1660, Carbolite, Bamford, Sheffield, UK) at 10 °C/min to 1500 °C, held for 4 h and then removed and water quenched (355105WQ).

Chunks of the water quenched frit (355105WQ) were ground into blocks 10 mm (length) $\times$7 mm (width) $\times$5 mm (depth), and polished finally with 1 μm diamond paste and cleaned. The glass frits (355105 and 355105WQ) were crushed and separately ground in a ball mill for 2 h, then screened to 125 μm sieve size to produce powders.

Particle size analysis

The ball milled powders (355105 and 355105WQ) were measured for the particle size and distribution using a mastersizer/E particle analyser (Malvern Instruments, UK). The powders were added to a circulating water bath at 37 °C that circulated through a cell and was exposed to a laser. The particle size was measured by spherical volume in the range 0.5–180 μm (100 mm lens).

Differential thermal analysis

Glass powder samples (355105) were evaluated using differential thermal analysis (DTA) to elucidate the crystallization kinetics, using a Labsys TG/DTA 1600 °C (Setaram Instruments, Caluire, France). Weighed powder samples were placed into platinum sample holders and an alumina standard was used as a reference material. Samples were run from 23 to 1200 °C at a rate of 5, 20 and 25 °C/min and similarly cooled at these rates.

Study of the crystallization kinetics

Samples of the glass powders were produced by mixing a weighed quantity of powder (0.80–0.90 g) with 3 ml of distilled water and compacting in a steel mould under two bar pressure for 1 min. After removal, the powder compacts (355105, 355105WQ) and glass blocks (355105WQ) were placed on platinum foils and heated in an electric furnace (RHF 1660, Carbolite, Bamford, Sheffield, UK) from 23 °C at a rate of 3 °C/min to 1120 °C. Specimens were withdrawn from the furnace at 650, 700, 750, 800, 850, 900, 950, 1000 and 1120 °C and quenched, in order to view the areas of nucleation and crystallization. Once this was assessed powder compacts (355105, 355105WQ) were heated from 23 °C at a rate 3 °C/min and held at 850, 900, 950, and 1120 °C for 10, 30, 60, 120 and 180 min and withdrawn and quenched.

X-ray diffraction analysis

In order to determine the phases in the materials studied the experimental glasses and heat treated glasses were ground into a powder for X-ray diffraction analysis (XRD). The samples were placed in the holder of a Siemens D5000 diffractometer and using flat plate geometry, data was collected from 5 to 110° 2θ, with a step size of 0.02° and a count time of 12 s. Cu Kα radiation was used (Kα_1 = 1.5406 Å, Kα_2 = 1.5444 Å). Data was collected using a scintillation counter and a graphite diffracted beam monochromator.

Structure refinement

Data were refined using General Structure Analysis Software (GSAS, Los Alamos National Laboratory, USA). Three potential phases could be present and a starting model for each was determined from the Inorganic Crystal Structure Database at the Daresbury Laboratories (Daresbury, UK). The model used for tetragonal leucite was based on the structural determination of Palmer et al. [29]. The starting model used was a space group I41/a with lattice parameters of a = 13.06 Å and c = 13.75 Å (1 Å = 10^{-10} m). For the cubic leucite phase a space group of IA-3D was used, with starting unit cell dimensions of a = 13.5 Å [30]. The sanidine K (Si_3 Al) O_8 (disordered) phase was modelled using a space group of C2/m (no12) with lattice parameters of a = 8.604 Å, b = 13.035 Å, c = 7.175 Å and beta = 116 degree angle [31]. For the refinement, peak shapes were modeled on a pseudo Voigt distribution and an asymmetry parameter was refined. Scattering factors for neutral atoms were assumed. Because of the complex nature of the background, due to amorphous material, twenty background parameters were used. A scale factor, four peak shape variables, cell parameters and a zero point correction were refined. Structural parameters were not refined. The unit cell dimensions were determined for each sample.

Secondary electron imaging

The specimens heat-treated in order to reveal the crystallization kinetics of the glasses (355105, 355105WQ) were embedded in epoxy and prepared

for secondary electron imaging (SEI). All specimens were polished with 1 μm followed by 0.3 μm alumina micropolish (Buehler, USA) and cleaned. Cleaning in alcohol for 30 s and water rinsing was carried out before ultrasonic cleaning for 3 min at 50 °C. Specimen etching was achieved using 0.1% hydrofluoric acid for 1 min, followed by water rinsing. Etched specimens were mounted on coded brass stubs and gold coated using a sputter coater (Balzers ScDo5o Bal-Tec, Liechtenstein), for 100 s at 40 mA. Secondary electron imaging was carried out with a field emission scanning electron microscope (JSM 6300F, Joel, Ltd, UK), using an accelerating voltage of 5 or 10 kV. One photomicrograph was taken per etched specimen so that the microstructures could be quantitatively assessed. Photomicrographs were scanned using a quantitative stereological image processing system (Magiscan M2, Applied Imaging Instruments, Sunderland, Tyne and Wear, UK) connected to a video camera, in order to confirm the percentage area leucite content and the area of any surface or crystallographic features.

Separate specimens (355105, 355105WQ glass blocks) were also carbon coated to allow elemental analysis. This allowed elemental analysis of crystalline and amorphous phases that could not be identified using X-ray diffraction. Energy dispersive X-ray analysis (EDS) was used on the carbon coated specimens in a scanning electron microscope (JSM 6300, Joel Ltd, UK), with both 10 and 20 kV.

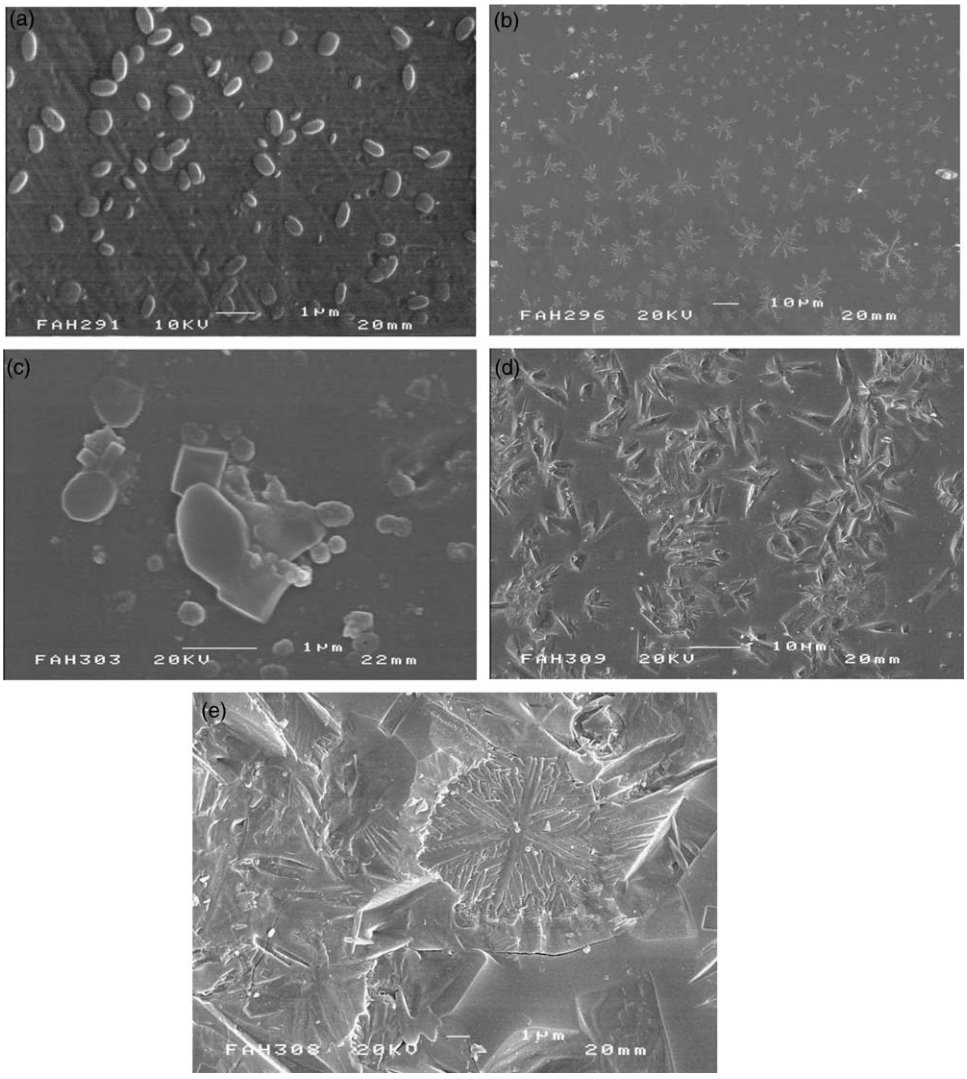

Figure 1 (a) SEM photomicrograph of the quenched glass block prior to heat treatment showing elliptical domains (×18000). (b) SEM photomicrograph of the quenched glass block withdrawn at 650 °C showing dendritic growth (×6500). (c) SEM photomicrograph of the quenched glass block withdrawn at 750 °C showing phase coarsening and crystallization (×19000). (d) SEM photomicrograph of the quenched glass block withdrawn at 850 °C showing sanidine crystals (×1300). (e) SEM photomicrograph of the quenched glass block withdrawn at 850 °C showing leucite and sanidine crystals (×5000).

Figure 2 Light microscope image of the 950 °C specimen displaying the morphology of leucite and sanidine crystals (×50).

Characteristic X-rays were acquired using a Pentafet detector and a beryllium window to give quantitative results, via an X-ray analysis program (Link eXLII, Oxford instruments, High Wycombe, UK). A dot map was used to quantify the elemental areas in several instances. Cobalt was used as a gain calibration during elemental quantitative analysis.

Light microscopy

Specimens were viewed in a light microscope (Olympus BX60, Olympus optical Co., Ltd, UK), before etching and gold coating and the images collected via a digital camera connected to a computer.

Results

Secondary electron imaging of the crystallization process

The 355105WQ glass (block) crystallization

The 355105WQ glass frit appeared transparent prior to crystallization. Photomicrographs illustrating the crystallization process for the 355105WQ polished glass blocks withdrawn over the temperature range 650–950 °C are shown in Figs. 1a–e and 2. Spherical and elliptical (mean (SD)) 0.1 (0.1) μm^2 phase separated areas were present in the quenched glass blocks (355105WQ), before heat treatment (Fig. 1a). The glass block withdrawn at 650 °C revealed tiny inclusions and areas of coarsening and dendritic growth (Fig. 1b). Signs of domain coarsening and primary crystallization were present on the 700 and 750 °C specimens (Fig. 1c). Crystallization was present at the grain boundaries or in the vicinity of coarsened phase separated areas (Fig. 1c). Increased signs of crystallization and coarsening were present for the 800 °C specimen. Extensive sanidine crystallization (platelets) occurred in the 850 °C specimen (Fig. 1d), together with a lower area fraction of leucite crystals (Fig. 1e). The 900 and 950 °C specimens produced leucite crystals together with a lower area fraction of sanidine crystals. Curling of the sanidine platelets was observed in the 850–950 °C temperature range. The morphology of these curved platelets can be clearly observed using light microscopy (Fig. 2). Extensive leucite crystallization was present for the 1000 °C specimen.

The 355105WQ and 355105 glass powder crystallization

Sanidine crystals (platelets) were visible in the 355105WQ powder samples for all holds at 850, 900 and 950 °C. Leucite crystals (mean (SD)) 4.2 (8.8) μm^2 (Table 1) and crystal and circumferential matrix microcracking were present for all of the 1120 °C samples (Fig. 3). The leucite crystals frequently appeared coarsened or coalesced, leading to an irregular shaped morphology. Possible phase separated areas were also present intermittently in the glassy matrix.

The 355105 glass frit appeared semi-transparent before the crystallization heat treatments. The glass powder (355105) withdrawn and quenched at 650 °C had signs of spherical phase separated areas and possible primary crystallization (Fig. 4a). Energy dispersive X-ray analysis (EDS) of the

Table 1 Crystalline content and leucite particle size of the 355105 and 355105WQ experimental glass-ceramics.

Experimental glass-ceramic	Crystalline component	Leucite area fraction (%)	Mean particle size ($\mu m^2 \pm$SD)	Particle size range (μm^2)
355105 ■	Tetragonal leucite[a]	15.9	1.1±0.7	0.02–3.9
355105 ▲	Tetragonal leucite	13.7	0.8±0.5	0.07–3.6
355105WQ ■	Tetragonal leucite	20.3	4.2±8.8	0.5–35.9

All Samples were ramped from 23 °C. ■ One-step heat treatment: (3 °C/min ramp to 1120/1 h hold); ▲ One-step heat treatment: (3 °C/min ramp to 1120/3 h hold).

[a] Trace amounts of cubic leucite were also present.

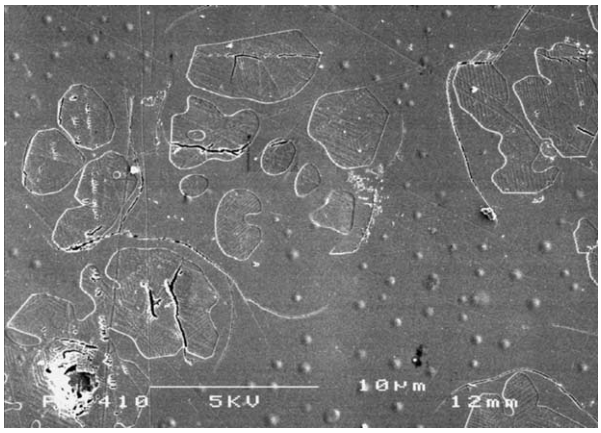

Figure 3 SEM photomicrograph showing leucite crystals and crystal and matrix microcracking in the 1120 °C/1 h hold, 355105WQ powder specimen (×3500).

spherical phase separated areas (Fig. 4c) and the glass matrix (Fig. 4d), together with an elemental dot map (Fig. 4b) illustrates calcium rich spherical phase separated areas.

The 355105 glass powder specimens heated from 23 °C at a rate of 3 °C/min to 1120 °C and quenched at temperatures of interest revealed signs of leucite at 800 °C, together with spherical phase separated areas. At 850 °C there was increased leucite growth, interspersed with glassy areas containing possible phase separated areas (Fig. 5a). A similar microstructure was evident for the 900 and 950 °C quenched specimens, but with increased leucite growth and signs of sanidine platelet growth. Sanidine platelet growth was increased for the 1000 °C quenched specimen, but with extensive leucite crystallization. The

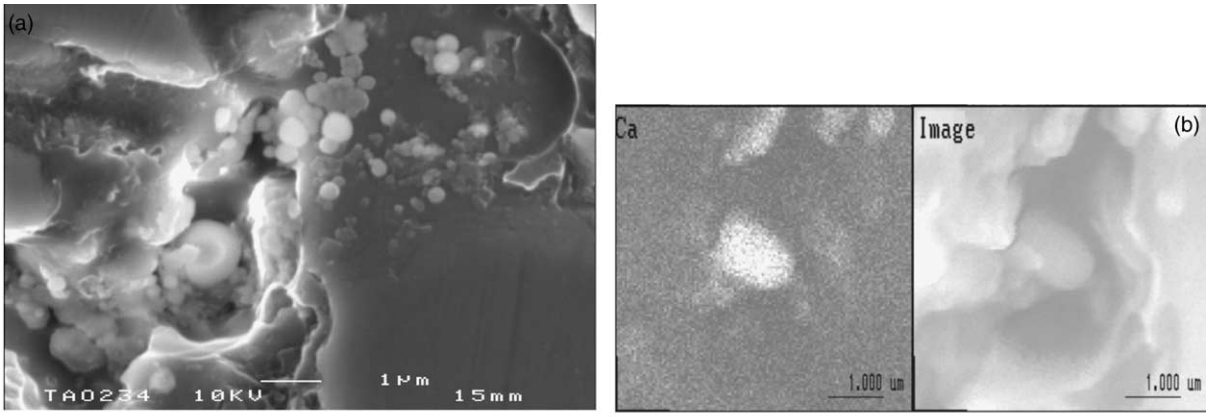

Elements	Element (%)	Fit index
Na	1.081	0.48
Mg	0.755	
Al	8.003	
Si	30.489	
K	15.614	
Ca	41.354	
Ti	0.648	
Cl	0.857	
S	1.201	

Elements	Element (%)	Fit index
Na	3.321	0.90
Mg	0.649	
Al	13.812	
Si	55.853	
K	21.765	
Ca	3.847	
Ti	0.536	
Cl	0.184	
S	0.030	

Figure 4 (a) SEM photomicrograph of the 355105 powder specimen quenched at 650 °C (×12000). (b) Elemental dot map showing calcium rich phase separated areas in the 355105 powder specimen quenched at 650 °C. (c) EDS spot analysis of the phase separated areas in the 355105 glass powder quenched at 650 °C. (d) EDS glass matrix spot analysis of the 355105 glass powder quenched at 650 °C.

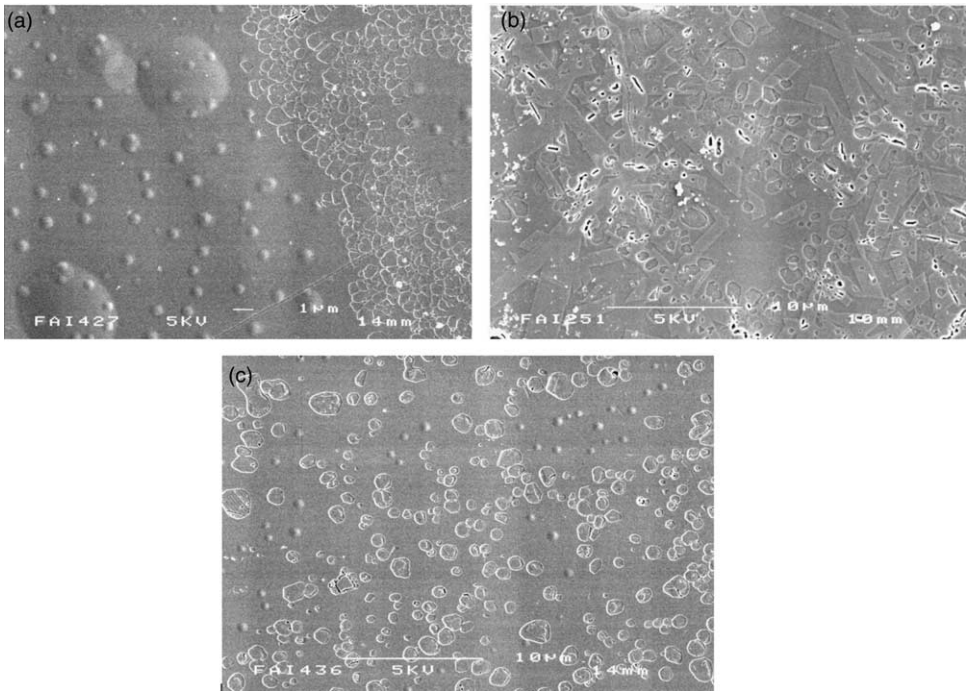

Figure 5 (a) SEM photomicrograph of leucite crystals and phase separation in a 355105 powder specimen heated from 23 °C at 3 °C/min and withdrawn at 850 °C (×5000). (b) SEM photomicrograph of leucite crystals and sanidine platelets in the 950 °C/1 h 355105 powder specimen (×3500). (c) SEM photomicrograph showing leucite crystals in the 1120 °C/1 h hold 355105 powder specimen (×3500).

1120 °C quenched specimen showed no signs of sanidine crystals, with a bulk leucite phase covering most of the microstructure. There were also still signs of spherical phase separation (<1 μm^2) in the glassy matrix.

The 355105 glass powder revealed the presence of leucite crystals in the glassy matrix at 850 °C for the 10 and 30 min holds (Fig. 5a). Sanidine platelets together with leucite crystals and areas of dendritic leucite growth were in evidence for the 1 h hold at 850 °C. Sanidine platelets were the only phase present for the 2 and 3 h holds at 850 °C. Sanidine and leucite crystals were visible for the 10, 30 min and 1 h holds at 900 °C. The 2 and 3 h 900 °C holds showed extensive sanidine crystallization. The 950 °C 10 and 30 min hold specimens produced leucite crystals and a lower area fraction of sanidine crystals. The 950 °C 1 h (Fig. 5b) and 2 h holds show an increase in sanidine crystallization at the expense of leucite, with extensive sanidine crystallization for the 3 h hold. All of the specimens held at 1120 °C produced leucite crystals and areas of glassy matrix only (Fig. 5c). Leucite crystals (mean (SD)) 1.1 (0.7) μm^2 (Table 1) were present in the specimens held at 1120 °C for 1 h.

Particle size analysis results

The results of the particle size analysis for 355105 and 355105WQ glass powders are listed in Table 2.

Differential thermal analysis results

Differential thermal analysis (DTA) data for the 355105 glass powder produced broad humps, rather than distinctive exothermic peak positions and the data was thought to be insufficient to calculate accurate activation energies or nucleation rates.

Table 2 The results of the particle size analysis for 355105 and 355105WQ glass powders.

Glass powder	Mean particle size, μm (50% below)	Mean particle size, μm (10% below)	Mean particle size, μm (90% below)
355105 glass (milled for 2 h)	5.39	1.11	23.47
355105WQ glass (milled for 2 h)	5.88	1.15	28.18

Table 3 The mean unit cell dimensions for the crystallized 355105WQ and 355105 glass powders after 1 h holds.

Glass-ceramic powder	Glass-ceramic	Mean a axis unit cell dimensions Å (SD)	Mean b axis unit cell dimensions Å (SD)	Mean c axis cell dimensions Å (SD)	Mean beta degree angle (SD)
355105WQ (850 °C)	Sanidine	8.5264 (0.0007)	12.9961(0.0012)	7.1458 (0.0006)	115.91 (0.007)
355105WQ (900 °C)	Sanidine	8.535 (0.0008)	13.0044 (0.0011)	701452 (0.0006)	115.89 (0.007)
355105WQ (950 °C)	Sanidine	8.5217(0.001)	12.9807 (0.002)	7.1445 (0.001)	115.93 (0.009)
355105WQ (1120 °C)	Tetragonal leucite	13.012 (0.003)	13.012 (0.003)	13.6344 (0.006)	90
355105 (1120 °C)	Tetragonal leucite	13.1879 (0.0006)	13.1879 (0.0006)	13.7489 (0.009)	90

All samples displayed were ramped from 23 °C at 3 °C/min and held for 1 h at the stated holding temperatures (1 Å = 10^{-10} m).

X-ray diffraction results

The X-ray diffraction pattern for the starting glass 355105 before heat treatment indicates a major amorphous glassy phase and some evidence of trace amounts of tetragonal leucite. The 355105WQ starting glasses indicated an amorphous glassy phase only. The X-ray diffraction results for the 355105WQ powder samples indicated a sanidine phase for all holds at 850, 900 and 950 °C. The 1120 °C held specimens resulted in a bulk tetragonal leucite phase only. The mean unit cell dimensions are listed in Table 3 for the crystallized 355105WQ and 355105 glass powders. The X-ray diffraction results for the 355105 glass powders held over the temperature range 850–1120 °C are listed in Table 4. X-ray diffraction traces are given for the phases identified (355105WQ, 355105) after 1 h holds for the 900 and 1120 °C temperatures (Figs. 6a–d). X-ray diffraction of the powder compacts (355105, 355105WQ) heated from 23 °C at a rate of 3 °C/min to 1120 °C and holding for 1, 2 and 3 h resulted in bulk tetragonal leucite phases (Tables 1 and 4). A trace cubic leucite phase was identified for the 355105 glass powder held at 1120 °C for 1 h.

Table 4 X-ray diffraction analyses of the crystallization process for the 355105 glass powder.

Temperature (°C)	Holding time (mins)	Phase major phase (MP) minor phase (M)
850	10	Tetragonal leucite
850	30	Tetragonal leucite (MP) + Sanidine (M)
850	60	Tetragonal leucite (MP) + Sanidine (M)
850	120	Sanidine
850	180	Sanidine
900	10	Tetragonal leucite
900	30	Tetragonal leucite(MP) + Sanidine (M)
900	60	Sanidine (MP) + Tetragonal leucite (M)
900	120	Sanidine (MP) + Tetragonal leucite (M)
900	180	Sanidine (MP) + trace Tetragonal leucite (M)
950	10	Tetragonal leucite (MP) + Sanidine (M)
950	30	Tetragonal leucite + Sanidine
950	60	Tetragonal leucite + Sanidine
950	120	Tetragonal leucite + Sanidine
950	180	Sanidine (MP) + trace leucite (M)
1120	10	Tetragonal leucite
1120	30	Tetragonal leucite
1120	60	Tetragonal leucite[a]
1120	120	Tetragonal leucite
1120	180	Tetragonal leucite

All samples were ramped from 23 °C to the holding temperatures at 3 °C/min before holding.
[a] A trace component that fitted cubic leucite was also identified.

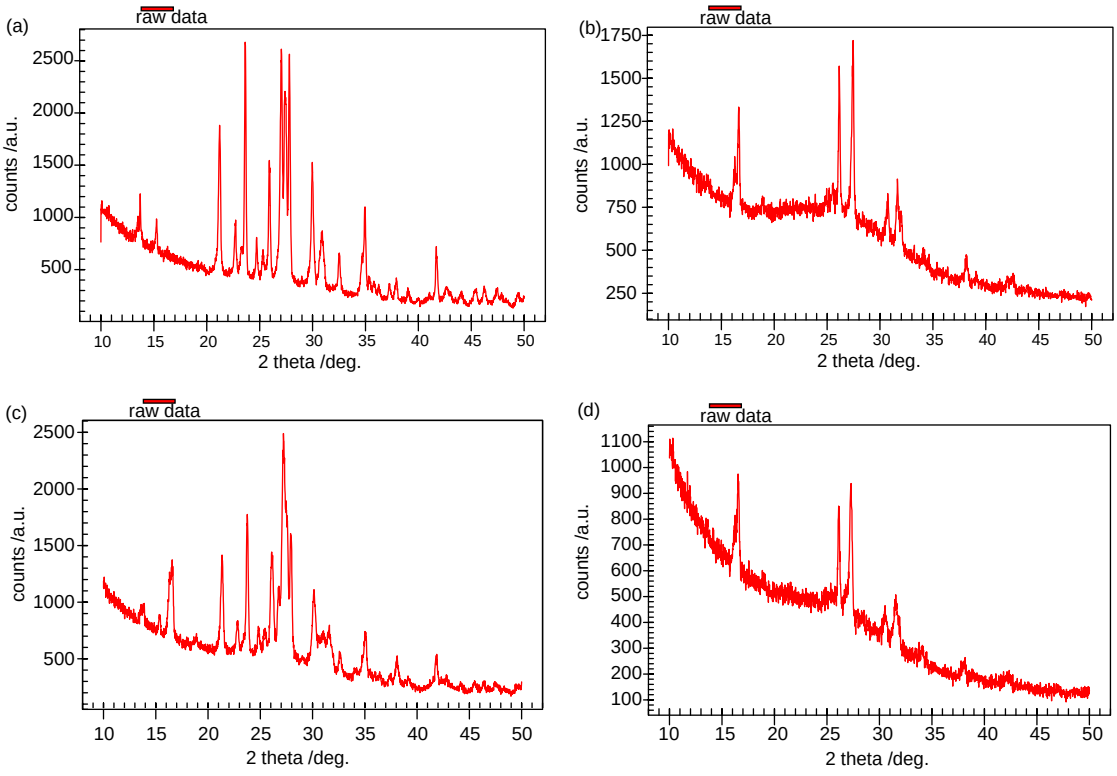

Figure 6 (a) The X-ray diffraction trace for the 900 °C/1 h hold, 355105WQ powder specimen. (b) The X-ray diffraction trace for the 1120 °C/1 h hold, 355105WQ powder specimen. (c) The X-ray diffraction trace for the 900 °C/1 h hold, 355105 powder specimen. (d) The X-ray diffraction trace for the 1120 °C/1 h hold, 355105 powder specimen.

Discussion

Scanning electron microscopy of the quenched glasses showed discreet elliptical and spherical domains in both the 355105WQ polished glass blocks (Fig. 1a), and both the 355105WQ and 355105 powder specimens (Fig. 4a). Energy dispersive X-ray analysis and an elemental dot map (Fig. 4b-d) revealed the presence of calcium rich spherical domains surrounded by more silica rich areas in the 355105 glass powder specimen. Amorphous phase separation may therefore be present, with high calcium aluminosilicate type phase separated areas. Immiscibility has been characterized in silicate glass forming systems, with the degree, connectivity, and composition of phase separated areas being related to the position on the immiscibility gap [32]. Further heat treatment caused the coalescence and coarsening of these areas (Ostwald ripening) and evidence of crystallization at the grain boundaries between the two glass phases. In particular, the precipitation of a platelet phase was preferential at this interface (Fig. 1c), which could have lowered the interfacial energy and provided an increased driving force for crystal nucleation [33]. The crystallization of a primary Sanidine platelet phase appeared to be associated with these calcium rich areas. Glass immiscibility in the form of phase separated CaO–P_2O_5 rich droplets were also previously thought to be instrumental in the bulk nucleation and crystallization of apatite in leucite-apatite glass-ceramics [34]. The phase separated areas in the glasses studied were calcium enriched compared to the surrounding glass which may have led to a region of increased mobility [35]. The formation of a diffusion zone around the phase separated areas or compositional shifts in matrix composition have been suggested as reasons for increased nucleation [36,37]. Increased activation energy of diffusion via phase separation could also have hindered coarsening, conserved nuclei, [38] and promoted fine grained crystallization. The reduction in the growth rate giving more time for the activation of nucleation sites. The crystallization of fine leucite crystals also occurred in areas adjacent to the phase separated areas (Figs. 1c and 5a) in the 355105WQ and 355105 glasses. The process of phase separation appeared to occur throughout the crystallization process in the 355105 and 355105WQ glass powders (ramped at 3 °C) up to 1120 °C.

Several authors have stressed the importance of titanium dioxide (TiO_2) as a nucleating agent in the base glass composition, [16,39] with significant

leucite crystallization at high (4-8 wt%) TiO_2 content [6]. Titanium dioxide was added to the 355105 (0.4 wt%) and 355105WQ (0.4 wt%) glass compositions and has been suggested as a sub-microscopic catalyst allowing the heterogeneous nucleation and growth of the major crystalline phase [40]. Amorphous phase separation may however, also be a consequence of high valence transition oxides like TiO_2 being displaced from the aluminosilicate network to form a separate phase with a divalent cation [41,38]. Evidence of this was not apparent in the studied glasses, but was identified by the present authors in compositions with higher TiO_2 content in subsequent work.

Leucite has previously been crystallized in alkali aluminosilicate glasses via controlled surface crystallization [39] and this was thought to be the dominant crystallization mechanism in the present glasses studied. Leucite crystal sizes in the range 0.1-1 μm were initiated from the surface in high (8 wt%) titanium containing alkali aluminosilicate glasses [16]. Simultaneous surface and volume leucite crystallization was however, also discussed in glass compositions with low K_2O content [16]. Tošić et al. [42] indicated surface leucite crystallization at particle sizes less than 0.075 mm and volume crystallization above this particle size in aluminosilicate glasses. The finding was complicated by the presence of secondary phases whose crystallization behavior was unknown. Further work is therefore necessary to confirm the above conclusions.

The early stages of bulk leucite growth have been observed as dendrites growing in four preferred crystallographic directions [42]. A diffusion controlled growth process that evolved at the smooth atomic-scale faceted crystal-glass interface was suggested. A change in dendrite shape due to the growth of secondary and tertiary fibrils and their ripening resulted in a highly organized tetragonal leucite structure. The 355105WQ glass block withdrawn at 650 °C (Fig. 1b) exhibited the growth of dendrites in six directions, which are crystallographically available for a cubic crystal. Further lateral growth and thickening of fibrils into uncrystallized areas between the main fibres were seen on the glass blocks withdrawn at 750 °C, 850 °C (Fig. 1e) and 950 (Fig. 2). Freiman et al. [43] described the slow lateral growth of arms into adjacent areas of uncrystallized melt as a secondary crystallization process. Freiman and Onada [44] confirmed Li^+ or Na^+ ions in glass maybe responsible for lowered viscosity and increased mobility affecting crystal morphology and growth. The alkali concentration at the grain boundaries and between the growing arms leading to secondary crystallization. Höland et al. [39] illustrated this type of dendritic leucite crystal growth from nucleating centres, inwards from the surface of monolithic glass samples. Faceted leucite morphology was observed in the heat treated 355105 glass powder. According to Uhlmann [45] this morphology may be related to a high entropy of fusion ($\Delta S_f > 4R$, where R is the gas constant), with diffusion controlled growth at the most closely packed interfaces becoming atomically smooth and faceted. Rearrangement at the growing interface and impurities in the melt are also controlling factors.

At 1120 °C leucite was the only crystalline phase detected in the glasses studied. The larger leucite crystals (mean (SD)) 4.2 (8.8) μm^2 (Table 1) in the 355105WQ glass had an irregular shaped morphology (Fig. 3) and microcracking was present in the surrounding glassy matrix after a one step heat treatment (3 °C/min ramp to 1120 °C/1 h hold). This was in complete contrast to the smaller (mean (SD)) 1.1 (0.7) μm^2 (Table 1) spherical leucite morphology in the 355105 glass and lack of matrix microcracking after the same heat treatment (Fig. 5c). An explanation may be an increased crystal growth rate in the 355105WQ glass linked with reduced glass viscosity caused by water quenching. Crystal nucleation and growth rates in silicate glasses previously increased in response to increased water content and reduced glass viscosity [46]. Mackert et al. [47] demonstrated that moisture might act as a glass modifier to enhance crystallization during a porcelain firing cycle. Trapped excess volume due to quenching or volatilization of elements during the glass making procedure may also be factors. Microcracking around the larger sized leucite crystals was not unexpected and has been reported for commercial leucite glass-ceramic materials [24].

A reduction in the leucite area fraction for the 355105 glass after a one-step heat treatment and holding for 3 h at 1120 °C was also evident (Table 1). Prolonged heating at 1120 °C may cause the dissolution of leucite and possible particle coalescence. Denry et al. [48] examined the crystallization of leucite glass-ceramics after prolonged heating at 1000–1100 °C and revealed a solution rim indicative of partial dissolution of leucite crystals. The morphology of the leucite crystals also changed to a more rounded structure than the unheated control material.

X-ray diffraction indicated that sanidine was present in the 355105WQ glass powder and blocks heat treated in the temperature range 850–950 °C, although signs of crystallization could be observed at lower temperatures. The heat treated 355105 glass powders in contrast, produced a tetragonal

leucite bulk phase initially and on further holding the coexistence of both tetragonal leucite and sanidine. Sanidine was then the bulk phase at the maximum holding time of 180 min (Table 4) within this temperature range. The differences in crystallization behavior of the powders may be associated with water quenching of the 355105WQ glass. Increasing the hydroxyl content may act as a modifier and break up the silicate network, reducing the viscosity and activation for viscous flow [38] as discussed earlier. Denry et al. [48] suggested sanidine crystallization occurred at reduced times and temperatures when glass viscosity was reduced by increased modifier content.

The precipitation of sanidine formed in the temperature range of 800–950 °C was previously identified in leucite reinforced glass-ceramics and the kinetics of phase transformation characterized by means of isothermal and continuous time-temperature-transformation diagrams [49]. Reconstructive transformations in order of descending temperature of leucite plus liquid, followed by leucite, sanidine and liquid and finally sanidine plus liquid may be studied using crystallization paths supplied by the K_2O–Al_2O_3–SiO_2 ternary phase diagram [4]. This crystallization behavior was characterized in the 355105 glass studied.

The unit cell dimensions of the sanidine crystallized in the 355105WQ glass (Table 3) were in the same range ($a=0.8524\pm0.0015$ nm, $b=1.30202\pm0.0004$ nm, $c=0.7165\pm0.0002$ nm, and beta$=116.02\pm0.01°$) as reported by Mackert et al. [50] for room temperature sanidine. The thermal expansion of sanidine was also estimated at 4.1×10^{-6} °C^{-1} (between 26.3 and 700 °C), which was substantially lower compared to leucite measured over the same range (28×10^{-6} °C^{-1}; 25–700 °C). The coexistence of a significant leucite-sanidine glass composite would lead to thermal expansion mismatches with the residual glass and deleterious microcracking.

The 355105 glass powder heat treated at a selected time and temperature (1120 °C for 1 h) produced a fine grained tetragonal leucite glass-ceramic, that has been shown to give improved mechanical properties compared to commercial glass-ceramic materials [51]. The glass-ceramic process described may also be a step to the production of fine grained glass-ceramics that benefit from less matrix microcracking and potentially better wear than current leucite reinforced glass-ceramics. Further studies have been carried out to elucidate the effects of increases in titanium dioxide to increase the leucite volume fraction and changes to the heat treatment schedules.

References

[1] Nathanson D. Principles of porcelain use as an inlay/onlay material. In: Garber DA, Goldstein RE, editors. *Porcelain and composite inlays and onlays, aesthetic posterior restorations*. Carol Stream, IL: Quintessence Publishing Co, Inc; 1994. p. 32–6.

[2] Wohlwend A, Schaerer P. The Empress technique for the fabrication of full ceramic crowns, inlays and veneers. *Quintessenz Zahntech* 1990;**16**:966–78.

[3] Mormann WH, Bindl A. The cerec 3—a quantum leap for computer-aided restorations: initial results. *Quintessence Int* 2000;**31**:699–712.

[4] Schairer JF, Bowen NL. The system K_2O–Al_2O_3–SiO_2. *Am J Sci* 1955;**253**:681–746.

[5] Binns DB. The chemical and physical properties of dental porcelain. In: McLean JW, editor. *Dental ceramics, Proceedings of the 1st international symposium on dental ceramics*. Chicago: Quintessence Pub., Co.; 1983. p. 41–56.

[6] Hermansson L, Carlsson R. On the crystallization of the glassy phase in whitewares. *Trans J Br Ceram Soc* 1978;**77**:32–5.

[7] Ibsen RL, Chadwick TC, Pritchard SA. Strong dental porcelain and method for its manufacture. US patent 5,009,709; 1991.

[8] Burk B, Burnett AP. Leucite containing porcelains and method of making same. US Patent 4101330; 1978.

[9] Weinstein M, Katz S, Weinstein AB. Fused porcelain to metal teeth. US Patent No. 3,052,982; 1962.

[10] Deer WA, Howie RA, Zussman J. Framework silicates. In: An introduction to the rock-forming minerals, 11th ed. London:Wiley; 1966, p. 281–317.

[11] Mackert Jr JR. Effects of thermally induced changes on porcelain-metal compatibility. In: Preston JD, editor. *Perspectives in dental ceramics, Proceedings of the fourth international symposium on ceramics*. Chicago: Quintessence Pub., Co.; 1988. p. 53–64.

[12] Mazzi F, Galli E, Gottardi G. The crystal structure of tetragonal leucite. *Am Mineral* 1976;**61**:108–15.

[13] Palmer C, Putnis A, Salje EKH. Twinning in tetragonal leucite. *Phys Chem Miner* 1988;**16**:298–303.

[14] Mackert JR, Butts MB, Fairhurst CW. The effect of the leucite transformation on dental porcelain expansion. *Dent Mater* 1986;**2**:32–6.

[15] Hermansson L, Carlsson R. High and low temperature forms of leucite. In: Proceedings, eighth international symposium on the reactivity of solids. Gothenberg, Sweden, Swedish Institute for Silicate Research; 1976. p. 541–5.

[16] Rouf MA, Hermansson L, Carlsson R. Crystallisation of glasses in the primary phase field of leucite in the K_2O–Al_2O_3–SiO_2 system. *Trans J Br Ceram Soc* 1978;**77**:36–9.

[17] Denry IL, Mackert Jr JR, Holloway JA, Rosenstiel SF. Effect of cubic leucite stabilisation on the flexural strength of feldspathic dental porcelain. *J Dent Res* 1996;**75**:1928–35.

[18] Piché PW, Obrian WJ, Groh CL, Boenke KM. Leucite content of selected porcelains. *J Biomed Mater Res* 1994;**28**:603–9.

[19] Mackert Jr JR, Russell CM. Leucite crystallisation during processing of a heat pressed dental ceramic. *Int J Prosthodont* 1996;**9**:261–5.

[20] Mackert Jr JR, Evans AL. Quantitative X-ray diffraction determination of leucite thermal instability in dental porcelain. *J Am Ceram Soc* 1991;**74**:450–3.

[21] Mackert Jr JR, Evans AL. Effect of cooling rate on leucite volume fraction in dental porcelains. *J Dent Res* 1991;**70**:37–139.

[22] Barreiro MM, Riesgo O, Vicente EE. Phase identification in dental porcelains for ceramo-metallic restorations. *Dent Mater* 1989;**5**:51–7.
[23] Shareef MY, Van Noort R, Messer PF, Piddock V. The effect of microstructural features on the biaxial flexural strength of leucite reinforced glass ceramics. *J Mater Sci: Mater Med* 1994;**5**:113–8.
[24] Cattell MJ, Knowles JC, Clarke RL, Lynch E. The biaxial flexural strength of two pressable ceramic systems. *J Dent* 1999;**27**:183–96.
[25] Fairhurst CW, Lockwood PE, Dingle RD, Thompson WO. The effect of glaze on porcelain strength. *Dent Mater* 1992;**8**: 203–7.
[26] Mackert Jr JR, Williams AL. Microcracks in dental porcelain and their behaviour during multiple firing. *J Dent Res* 1996; **75**:1484–90.
[27] Cattell MJ, Clarke RL, Lynch E. The transverse strength, reliability and microstructural features of four dental ceramics-part 1. *J Dent* 1997;**25**:399–407.
[28] Metzler KT, Woody RD, Miller AW, Miller BH. In vitro investigation of the wear of human enamel by dental porcelain. *J Prosthet Dent* 1999;**81**:356–64.
[29] Palmer DC, Dove MT, Ibberson RM, Powell BM. Structural behavior, crystal chemistry and phase transitions in substituted leucite: high resolution neutron diffraction studies. *Am Miner* 1997;**82**:16–29.
[30] Dove MT, Cool T, Palmer DC, Putnis A, Salje EKH, Winkler B. On the role of Al–Si ordering in the cubic-tetragonal transition of leucite. *Am Miner* 1993;**78**:486–92.
[31] Scheel HJ. Lead feldspar. *Zeitschrift für kristallographie* 1971;**133**:264–72.
[32] Seward TP, Uhlmann DR, Turnbull D. Development of two-phase structures in glasses with special reference to the system BaO–SiO_2. *J Am Ceram Soc* 1968;**51**:634–43.
[33] Uhlmann DR. General discussion. *Trans Faraday Soc* 1970; **50**:223–34.
[34] Szabó I, Nagy B, Völksch G, Höland WH. Structure, chemical durability and microhardness of glass-ceramics containing apatite and leucite crystals. *J Non-Cryst Solids* 2000;**272**: 191–9.
[35] Ohlberg SM, Golob HR, Strickler DW. Crystal nucleation by glass in glass separation. In: Symposium on nucleation and crystallisation in glasses and melts, Columbus, OH: Ceramic Society; 1962. p. 55–62.
[36] James PF. Nucleation in glass forming systems—a review. In: Simmons JH, Uhlmann DR, Beall GH, editors. In: *Advances in ceramics, nucleation and crystallisation in glasses*, 4. Columbus, OH: The American Ceramic Society; 1982. p. 14–48.
[37] Tomozawa M. Liquid phase separation and crystal nucleation in Li_2O–SiO_2 glasses. *Phys Chem Glasses* 1972;**13**:161–6.
[38] McMillan PW. *Glass-ceramics*. 2nd ed. London: Academic Press Inc.; 1979 p. 34–122.
[39] Höland WH, Frank M, Rheinberger V. Surface crystallization of leucite in glass. *J Non-Cryst Solids* 1995;**180**:292–307.
[40] Stookey SD. Catalysed crystallization of glass in theory and practice. *Ind Eng Chem* 1959;**51**:805–8.
[41] Beall GH, Duke DA. Transparent glass ceramics. *J Mater Sci* 1969;**4**:340–3352.
[42] Tošić MB, Mitrović MM, Dimitrijević RZ. Crystallization of leucite as the main phase in aluminosilicate glass with low fluorine content. *J Mater Sci* 2000;**35**:3659–67.
[43] Freiman SW, Onada GY, Pincus AG. Spherulitic crystallization in glasses. In: Hench LL, Freiman SW, editors. *Advances in nucleation and crystallisation in glasses*. Columbus, OH: The American Ceramic Society, Inc.; 1971. p. 141–50.
[44] Freiman SW, Onada GY. Effect of akali ions on the crystallization of BaO $5SiO_2$ glass. *J Am Ceram Soc* 1997; **80**:3263–7.
[45] Uhlmann DR. Crystal growth in glass forming systems—a review. In: Hench LL, Freiman SW, editors. *Advances in nucleation and crystallization in glasses*. Columbus, OH: American ceramic society, Inc.; 1971. p. 91–112.
[46] James PF. Nucleation in glass forming systems—a review. In: Simmons JH, Uhlmann DR, Beall GH, editors. In: *Advances in ceramics, nucleation and crystallisation in glasses*, 4. Columbus, OH: The American Ceramic Society; 1982. p. 14–48.
[47] Mackert Jr JR, Williams AL, Ergle JW, Russell CM. Water enhanced crystallisation of leucite in dental porcelain. *Dent Mater* 2000;**16**:426–31.
[48] Denry IL, Holloway JA, Colijn HO. Phase transformations in a leucite-reinforced pressable dental ceramic. *J Biomed Mater Res* 2001;**54**:351–9.
[49] Barreiro MM, Vicente EE. Kinetics of isothermal phase transformations in a dental porcelain. *J Mater Sci Mater Med* 1993;**4**:431–6.
[50] Mackert Jr JR, Twiggs SW, Williams AL. High-temperature X-ray diffraction measurement of sanidine thermal expansion. *J Dent Res* 2000;**79**:1590–5.
[51] Cattell MJ, Chadwick TC, Knowles JC, Clarke RL, Lynch E. Flexural strength optimization of a leucite reinforced glass ceramic. *Dent Mater* 2001;**17**:21–33.